Breitenlohner-Freedman Bound on Hyperbolic Tilings

Pablo Basteiro, Felix Dusel, Johanna Erdmenger,[*] Dietmar Herdt, Haye Hinrichsen, René Meyer, and Manuel Schrauth

Julius-Maximilians-Universität Würzburg (JMU), Institute for Theoretical Physics and Astrophysics and Würzburg-Dresden Excellence Cluster ct.qmat, Am Hubland, 97074 Würzburg, Germany

We establish how the Breitenlohner-Freedman (BF) bound is realized on tilings of two-dimensional Euclidean Anti–de Sitter space. For the continuum, the BF bound states that on Anti–de Sitter spaces, fluctuation modes remain stable for small negative mass squared m^2. This follows from a real and positive total energy of the gravitational system. For finite cutoff ε, we solve the Klein-Gordon equation numerically on regular hyperbolic tilings. When $\varepsilon \to 0$, we find that the continuum BF bound is approached in a manner independent of the tiling. We confirm these results via simulations of a hyperbolic electric circuit. Moreover, we propose a novel circuit including active elements that allows us to further scan values of m^2 above the BF bound.

Introduction.—The AdS/CFT correspondence [1–3], also known as holography, maps gravitational theories in $(d + 1)$-dimensional hyperbolic Anti–de Sitter (AdS) spacetimes to strongly coupled conformal field theories (CFTs) without gravity in d dimensions, defined on the AdS boundary. The AdS/CFT duality provides a precise map between CFT operators and AdS gravity fields, which is of great significance both for fundamental aspects of quantum gravity [4] and for applications to strongly correlated condensed matter systems [5].

Motivated by the goal to provide a new example of holographic duality, as well as possible realizations in tabletop experiments, in this Letter we report novel insights in this direction for discretized systems. A prime candidate is a scalar field defined on discretizations of AdS space via regular hyperbolic tilings (see Fig. 1) [6,7], which have been recently investigated using methods from lattice gauge theory in Refs. [8–11]. These works consider discretization schemes for the scalar action, the Laplace operator, and lattice bulk propagators, finding good agreement of the scaling behavior of correlation functions with analytic continuum results.

The physics of hyperbolic tilings has recently been studied in the context of condensed matter physics [12], circuit quantum electrodynamics [13–15], and topolectric circuits [16–18]. These works focus on the spectrum of tight-binding Hamiltonians on hyperbolic lattices and their

realization based on coupled waveguide resonators [12,14,15] or classical nondissipative linear electric circuits (topolectric circuits). Time-resolved measurements of wave propagation in hyperbolic space have been achieved in such architectures [17].

It remains an open question, though, how to establish a duality in the sense of a map between bulk and boundary theories for hyperbolic tessellations. Steps in this direction were taken in Refs. [19,20] using modular discretizations and in Ref. [21] via tensor networks on hyperbolic buildings. In this Letter, we focus on hyperbolic tilings as a discretization scheme instead. The starting point is one of the key results of the continuum AdS/CFT correspondence, namely the relation between the mass m of a scalar field in the bulk and the scaling dimension Δ of its dual
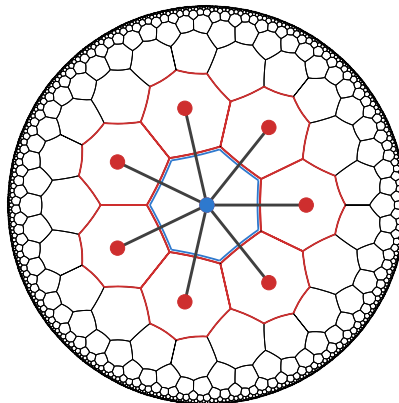

FIG. 1. Hyperbolic $\{7,3\}$ tiling in the Poincare disk representation. For the central node, the stencil of the discretized Laplace-Beltrami operator is highlighted. Red sites carry constant weights $w^{(7,3)}$, whereas the central node (blue) is weighted by $-7w^{(7,3)}$.

operator on the boundary, $\Delta(\Delta - d) = m^2\ell^2$, with ℓ being the AdS radius and d the boundary spacetime dimension [2]. This is determined by the asymptotic boundary behavior of the solutions of the Klein-Gordon equation in AdS space. Conformally transforming AdS space into flat space, the scalar field experiences a shift of its mass squared to $m^2\ell^2 + d^2/4$. Thus, there is a stable potential minimum for the field if $m^2\ell^2 > -d^2/4$, i.e., even for small negative mass squared. This is the *Breitenlohner-Freedman* (BF) bound [22–24].

In this Letter, we determine how the BF bound is realized in discrete holographic setups and how it manifests itself on finite-sized architectures accessible through simulation and experiment. We establish the BF bound for hyperbolic tessellations by first analyzing the properties of the continuum analytical solutions in the presence of a finite cutoff. This cutoff can be chosen arbitrarily and is required because only finite tilings, which do not cover the entirety of hyperbolic space, can be experimentally and numerically realized. In particular, this cutoff is independent of the Schläfli parameter $\{p, q\}$ characterizing a regular hyperbolic tiling with q regular p-gons meeting at each vertex. Defining a scalar field on the vertices, we numerically solve the associated equations of motion on several tilings, finding excellent agreement with results from continuum holography. We find that the stability bound of a scalar field defined on large enough $\{p, q\}$ hyperbolic tilings coincides with the continuum BF bound, independently of p and q. Our analysis extends previous investigations [13,15,17] of the eigenvalue problem of the discrete Laplacian on these tilings. In particular, we use insights from holography, such as the presence of non-normalizable modes, to provide solutions for masses squared above the BF bound, thus beyond the standard spectrum of the Laplacian. Moreover, we propose a novel electric circuit, in the spirit of topolectric circuits [26,27], to access these new mass-squared values in experiment.

Equations of motion on EAdS_2.—In order to investigate the physics of the BF bound for hyperbolic tilings, we consider one of the simplest continuum systems admitting a holographic duality, a free massive scalar field Euclidean AdS_2 (EAdS_2), with the induced metric

$$ds^2 = g_{\mu\nu}dx^\mu dx^\nu = \frac{\ell^2}{\cos^2(\theta)}(d\theta^2 + \sin^2(\theta)d\phi^2). \quad (1)$$

Here, ℓ is the curvature radius of EAdS_2, and $\theta \in [0, (\pi/2))$, $\phi \in [0, 2\pi)$. The asymptotic boundary of EAdS_2 is at $\theta = \pi/2$, corresponding to an infinite geodesic distance from the origin $\theta = 0$. The scalar field action

$$S = \frac{1}{2}\int d^2x\sqrt{g}(\partial^\mu\Phi\partial_\mu\Phi + m^2\Phi^2) \quad (2)$$

yields as equation of motion the Klein-Gordon equation [28]

$$0 = \frac{1}{\sqrt{g}}\partial_\mu(\sqrt{g}g^{\mu\nu}\partial_\nu\Phi) - m^2\Phi \equiv (\Box - m^2)\Phi \quad (3)$$

$$= \frac{1}{\ell^2}\cos\theta\cot\theta\frac{\partial}{\partial\theta}\left(\sin\theta\frac{\partial\Phi}{\partial\theta}\right) - m^2\Phi(\theta), \quad (4)$$

with $\Box$ the Laplace-Beltrami operator on EAdS_2. The second equality in Eq. (4) holds for a purely θ-dependent field configuration $\Phi(\theta)$ with no angular dependence. Equation (4) admits analytic solutions in terms of hypergeometric functions Eq. (S.2) in the Supplemental Material [29], parametrized by two integration constants, which can be related by the regularity boundary condition $\Phi'(0) = 0$. Asymptotically near the boundary at $\theta = \pi/2$, the two fundamental solutions behave as

$$\Phi(\theta) \simeq A(\cos\theta)^{1-\Delta} + B(\cos\theta)^\Delta, \quad (5)$$

where $\Delta = \frac{1}{2} + \sqrt{\frac{1}{4} + m^2\ell^2}$ is the scaling dimension of the boundary operator O holographically dual to Φ. In AdS/CFT, the terms in Eq. (5) are denoted as *non-normalizable* and *normalizable* modes, respectively. Imposing suitable boundary conditions at $\theta = (\pi/2)$ [37], the coefficient B of the normalizable mode is identified with the vacuum expectation value of the dual operator O, while the coefficient A of the non-normalizable mode determines its source J. In spatial dimension $d = 1$ and for masses of the scalar field

$$m^2\ell^2 < -\frac{1}{4}, \quad (6)$$

the scaling dimension Δ of the dual operator becomes complex. In the CFT, this indicates a breakdown of unitarity. In the AdS bulk, it implies that the energy of the scalar field,

$$E = \int d\theta\,\cos(\theta)^{2\Delta}((\partial_\theta\tilde{\Phi})^2 + \Delta^2\tilde{\Phi}^2), \quad (7)$$

ceases to be a real and positive quantity [29]. Here, we have used the ansatz $\Phi(\theta) = (\cos\theta)^\Delta\tilde{\Phi}(\theta)$ [22,23,38]. After quantization, this denotes an instability of the system toward a new, true ground state [39]. The reality condition on Δ implies $m^2\ell^2 \geq -\frac{1}{4}$. This is the Breitenlohner-Freedman stability bound [22,23] and is a key element of AdS/CFT.

We now analyze the implications of a finite cutoff for the analytical solutions. Regularity at the origin is imposed through von Neumann boundary conditions at $\theta = 0$. Introducing a finite radial cutoff $\varepsilon \ll 1$, such that Dirichlet boundary conditions are imposed at $\theta_c = \pi/2 - \varepsilon$ via $\Phi(\theta_c) = 1$, leads to a rescaling of the solutions. We
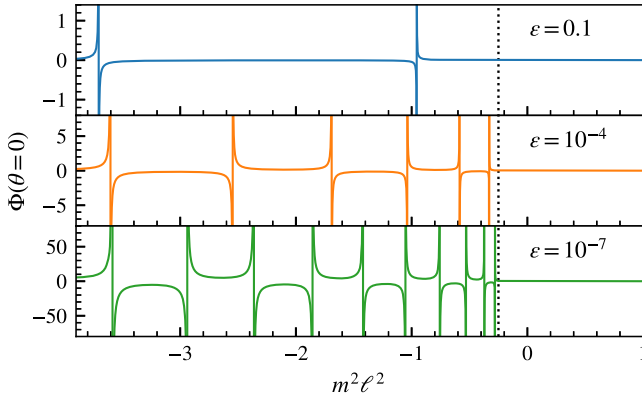
FIG. 2. Field amplitude at the origin for different cutoff values ε. We observe *Umklapp points* appearing at any finite cutoff, the rightmost of which can be used as an indicator of unstable solutions. For smaller cutoffs, the Umklapp points become denser and converge toward the continuum BF bound (dotted line).

solve Eq. (4) subject to these boundary conditions and find that, above the BF bound, solutions have no zeros in the regime $\theta \in [0, (\pi/2))$. Below the BF bound, however, solutions develop an infinite set of zeros [29].

At specific values of the mass squared $m^2\ell^2$ and cutoff ε, we observe a singular behavior of the solutions, characterized by discontinuous jumps of the field amplitude, as presented in Fig. 2. These only appear below the BF bound and are a result of the cutoff coinciding with a zero of the solution associated to the given value of $m^2\ell^2$, thus making the rescaling factor diverge. We denote these pairs $(m^2\ell^2, \varepsilon)$ as *Umklapp points*. The position of the first Umklapp point below $m^2\ell^2 = -\frac{1}{4}$, corresponding to the zero which is furthest into the bulk, can be used as an indicator for the unstable regime. More precisely, when the cutoff is removed, the value of the mass squared for which this zero first appears corresponds to the BF stability bound. The analytical derivation of the solutions to the Klein-Gordon equation (4) at a finite cutoff ε provided in Ref. [29] allows for an exact tracking of this first Umklapp point for different cutoffs. This provides a reference behavior, shown in black in Fig. 3, to which we compare our numerical findings.

Regular hyperbolic tilings of $\mathbb{D}^2$.—EAdS$_2$ is isomorphic to the Poincaré disk model of hyperbolic space $\mathbb{D}^2$, which can be naturally discretized by *regular hyperbolic tilings* [6,7]. These preserve a large subgroup, known as a *Fuchsian group of the first kind*, of the isometry group PSL$(2, \mathbb{R})$ of EAdS$_2$ [40,41], making them promising candidates for setting up a discrete holographic duality. Hyperbolic tilings are characterized by their Schläfli symbol $\{p, q\}$, with $(p-2)(q-2) > 4$, denoting a tiling with q regular p-gons meeting at each vertex. The $\{7, 3\}$ hyperbolic tiling and its dual $\{3, 7\}$ tiling are shown in Fig. 1 as an example. Since hyperbolic space introduces a length scale through its radius of curvature ℓ, the edge
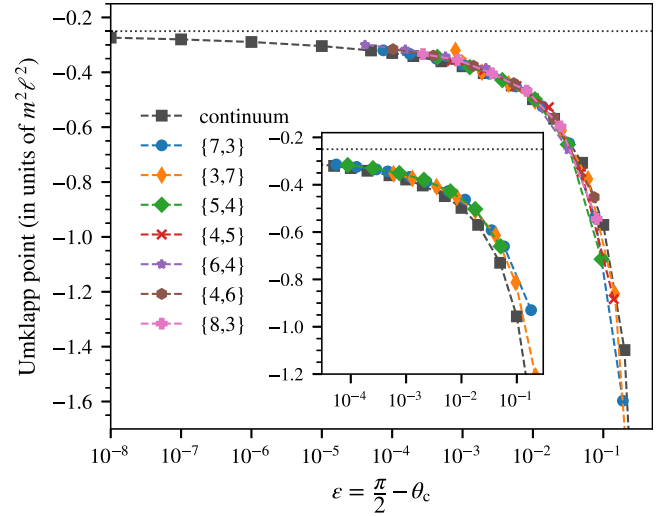

FIG. 3. First Umklapp point for various hyperbolic tilings and radial cutoffs θ_c. For small ε, the curves tend toward the continuum bound $m^2\ell^2 = -1/4$, indicated by the dotted horizontal line. Inset: corresponding results from our hyperbolic electric circuit simulations.

lengths of hyperbolic polygons are fixed quantities, depending only on the Schläfli parameters p and q [42]. Their geodesic length $\theta^{(p,q)}$ in units of ℓ can be computed via the Poincaré metric [Eq. (1)] and can be interpreted as a fixed lattice spacing that cannot be tuned. We compute $\theta^{(p,q)}$ for several p and q in Ref. [29]. In general, this makes a continuum limit of $\{p, q\}$ tilings in the usual way impossible. Nevertheless, we provide evidence that regular hyperbolic tilings indeed preserve some properties of the continuum scalar field theory, indicating that they are a good approximation of continuum EAdS$_2$.

While the entire EAdS$_2$ space can be filled with an infinite $\{p, q\}$ tiling, numerical simulations and experimental setups can only be finite sized. The truncation of the tiling to a finite number of layers is equivalent to the introduction of a finite cutoff as mentioned earlier. Given the jagged structure of the tiling's boundary at any finite layer, an effective uniform radial cutoff needs to be drawn. This allows for a direct comparison of the Umklapp points observed in numerical simulations on the truncated tilings with the analytical solutions derived in Ref. [29].

Numerical methods.—The central ingredient for our numerical analysis of the Klein-Gordon equation on $\{p, q\}$ hyperbolic tilings is a suitable discretization, denoted by $\tilde{\Box}$, of the Laplace-Beltrami operator. Its action on a scalar function $\Phi(\theta, \phi)$, represented on the tiling by discrete values $\Phi_j = \Phi(\theta_j)$, can be written as

$$(\tilde{\Box}\Phi)_j = \sum_{k|j} w_{jk}\ell^{-2}(\Phi_k - \Phi_j), \qquad (8)$$

where $k|j$ denotes the summation over the q neighboring sites k of site j. In order to determine the weight factors w_{jk},

we implement the following method devised from the established approximation of lattice operators by finite difference quotients. Given that all cells in a hyperbolic tiling are isometric, it is clear that all weights in the stencil have to be equal, i.e., $w_{j,k} \equiv w$ (cf. right panel of Fig. 1), which allows us to write the lattice operator formally as a matrix

$$\tilde{\Box} - m^2 \equiv w\ell^{-2}(A - G) + M, \qquad (9)$$

acting on a vector of function values $\Phi = (\Phi_0, \Phi_1, \ldots)$. Here, A and G denote the adjacency and degree matrix of the tiling graph and $M = \text{diag}(-m^2)$. In order to calculate the weight w, recall the approximation of a 1D second derivative by finite differences $\tilde{\partial}_x^2 \chi(x) = w[\chi(x - h) - 2\chi(x) + \chi(x + h)]$. First, we determine a test function $\chi(x)$ such that $\partial_x^2 \chi(x) = 1$, in this case $\chi(x) = \frac{1}{2}x^2$. Applying the discretized derivative to this function yields $\tilde{\partial}_x^2 \chi(x) = h^2 w$; hence $w = h^{-2}$. Note that unlike this case of a Cartesian hypercubic lattice, the hyperbolic lattice spacing h is fixed, as discussed above.

We now apply this procedure to the stencil on the hyperbolic lattice. First, we determine a radially symmetric test function $\chi(\theta)$ such that

$$\Box \chi(\theta) = \frac{1}{\ell^2}(\cos^2\theta \cot\theta \partial_\theta + \cos^2\theta \partial_\theta^2)\chi(\theta) = 1. \quad (10)$$

A possible solution is

$$\chi(\theta) = \ell^2 \ln\left(1 + \frac{1}{\cos\theta}\right). \qquad (11)$$

Applying $\tilde{\Box}$ to this function on the central site of the tiling (cf. right panel of Fig. 1) yields

$$\tilde{\Box}\chi(0) = pw(\chi(\theta^{(p,q)}) - \chi(0)) = 1. \qquad (12)$$

Solving for w, the weight factors can be obtained for every $\{p, q\}$ and are listed in Ref. [29].

Numerical results.—Given the lattice Laplacian, the continuum Klein-Gordon equation on a constant time slice can be expressed on the finite hyperbolic tiling as

$$\tilde{\Box}\Phi - m^2\Phi = 0 \quad \text{for } \theta < \theta_c,$$
$$\Phi(\theta) = \Phi_c \quad \text{for } \theta = \theta_c \qquad (13)$$

where the boundary condition is implemented by assigning constant values to sites outside the radial cutoff θ_c.

Solving the discretized boundary value problem [Eq. (13)] requires iterative matrix methods [43,44] already for medium system sizes. It has to be taken into account that for negative m^2 exceeding a certain threshold, most standard solvers tend to be unstable due to the lattice

operator $\tilde{\Box} - m^2$ becoming indefinite in this parameter regime [45]. A class of algorithms which can handle indefinite, sparse linear systems are so-called Krylow subspace methods [46]. In particular, we use both the GMRES (generalized minimum residual) [47] and BiCGSTAB (biconjugate gradient stabilized) gradient stabilized [48] methods to solve Eq. (13) and extract the positions of the Umklapp points. The results from both algorithms are fully compatible and presented in Fig. 3 for various hyperbolic tilings [49] and values of the cutoff. We find that all curves nicely converge toward $m^2\ell^2 = -1/4$ for $\varepsilon \to 0$, thus yielding the correct infinite volume limit and marking the main result of this Letter.

We expect that the universal behavior for all p and q displayed in Fig. 3 originates from a group-theoretic argument as follows. For Fuchsian groups of the first kind, which describe the isometries of $\{p, q\}$ tilings, it is known that the boundary limit set is the circle S^1 [21,40]. For infinite tilings, this implies conformal invariance of the boundary theory. The BF bound is the mass-squared threshold at which the scaling dimension Δ of the CFT operator dual to the bulk scalar field becomes complex, as can be seen from the definition of Δ below [Eq. (5)]. Thus, the asymptotic value of the first Umklapp point must be the same for all p and q as $\varepsilon \to 0$. In addition, our numerical results of Fig. 3 indicate that even for finite cutoff, where the Fuchsian symmetry is broken, the universality of the $\varepsilon \to 0$ behavior is preserved for all p and q.

Hyperbolic electric circuits.—We further propose an experimental realization of the BF bound in a suitable electric circuit. We are motivated by topolectric circuits [16], which are a platform based on circuits of capacitors and inductors which are engineered to realize a plethora of models exhibiting topological states of matter [26,27,50]. Specifically, let us consider a circuit on a hyperbolic tiling as shown in Fig. 4. On the vertices of the tiling we attach grounded capacitors C and connect them via identical inductors L along the polygon edges. Note that our
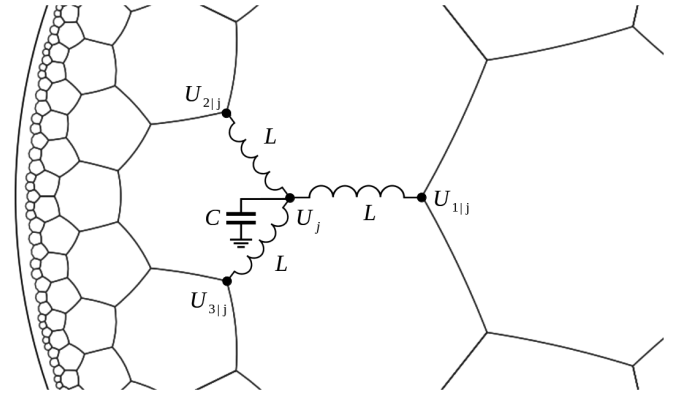

FIG. 4. Section of the hyperbolic electric circuit. The structure is repeated at every vertex in the lattice.

construction differs from that in Ref. [17] in that we exchange capacitors and inductors. This is necessary because only then the site voltage U_j represents the scalar field ϕ_j. In this network, the voltage U_j at site j is related to the capacitor current by $I_j = C\dot{U}_j$ while the voltage differences between neighboring sites k of j are related to the induced current by $(U_k - U_j) = L\dot{I}_{jk}$. According to Kirchhoff's laws, the time evolution of the voltage at site j is given by

$$\ddot{U}_j = \frac{1}{LC}\sum_{k|j}(U_k - U_j). \tag{14}$$

The oscillatory eigenmodes $U_j(t) = u_j e^{i\omega t}$ are determined by the system of equations

$$-\omega^2 U_j = \frac{1}{LC}\sum_{k|j}(U_k - U_j) = \frac{w^{(p,q)}}{LC}\tilde{\Box}U_j, \tag{15}$$

where in our case, the weights are constant $w_{jk} = w^{(p,q)}$ as discussed above. By identifying

$$-m^2\ell^2 = \omega^2 \frac{LC}{w^{(p,q)}}, \tag{16}$$

the electric circuit provides a realization of the discretized Klein-Gordon equation for $m^2\ell^2 < 0$ [51].

The first Umklapp point corresponds to the lowest eigenfrequency of the circuit, which represents the finite gap in the negative-definite eigenspectrum of the hyperbolic Laplacian [15]. Since the circuits described above contain only passive elements, they can only realize the regime of negative mass squared. This is however precisely the regime where according to Eq. (7), solutions to Eq. (4) are unstable within the AdS/CFT correspondence. For electric circuits to access the regime of m^2 above the BF bound, thus realizing non-normalizable solutions [Eq. (5)] essential for holography, the implementation of active electrical elements is required. Such elements were introduced in Ref. [52] in the context of topolectric circuits. We propose to use negative impedance converters to achieve negative values of L or C on the rhs of Eq. (16).

In order to systematically locate the eigenmodes of the passive circuit, we apply a driving alternating current at the central node and integrate the system of Eq. (15) over time using an explicit fourth-order Runge-Kutta method. Details of our numerical analysis are presented in Ref. [29]. Once the fundamental mode of the system is found, the corresponding negative mass squared can be extracted according to Eq. (16). These resonances (eigenfrequencies of the circuit) are a physical manifestation of the Umklapp points introduced above. Performing this analysis for several different hyperbolic tilings [49] and finite cutoff radii, we are able to locate the positions of the lowest eigenfrequency. Similarly to our analysis of the Umklapp points, we are able to find the instability threshold on the tiling by

tracking the position of the first resonance frequency of the circuit as the cutoff is removed. Again, we find an excellent agreement with the continuum prediction, as shown in the inset of Fig. 3. Our analysis thus shows how the BF bound can be experimentally realized on hyperbolic electric circuits.

Conclusions.—For the first time, we have identified the implications of the Breitenlohner-Freedman bound for discrete regular tilings of hyperbolic space. Notably, we find universal behavior of the instabilities for all $\{p, q\}$ discretizations, even for finite cutoff. In particular, we find excellent agreement between the positions of the Umklapp points as obtained via numerical simulations of the scalar field on several different $\{p, q\}$ tilings with the analytical solutions of the Klein-Gordon equation on EAdS$_2$. Moreover, for a specific hyperbolic electric circuit we show how the resonance frequencies are a manifestation of the Umklapp points. Simulations of the circuit dynamics also show excellent agreement with the analytical data by yielding the same dependence of the resonances on the cutoff size. Both these results confirm the universal behavior. Furthermore, we suggest how to adapt the electrical circuits in order to realize mass-squared values above the BF bound. Such circuit realizations will make regular hyperbolic tilings excellent candidates for bringing aspects of AdS/CFT to the laboratory.

The EAdS$_2$ manifold considered here describes a constant time slice of the larger AdS$_{2+1}$ spacetime. It would be interesting to generalize our analysis to a Lorentzian setting involving time, for instance by adding a temporal leg to the vertices of the tilings and equipping them with radius-dependent weights (see also Ref. [11] for a first attempt in this direction). In practice, this can be implemented by locally modifying L and C on the hyperbolic electric circuit. We leave this for future work.

[*] erdmenger@physik.uni-wuerzburg.de

[1] J. M. Maldacena, The large N limit of superconformal field theories and supergravity, Adv. Theor. Math. Phys. **2**, 231 (1998).

[2] S. S. Gubser, I. R. Klebanov, and A. M. Polyakov, Gauge theory correlators from noncritical string theory, Phys. Lett. B **428**, 105 (1998).

[3] E. Witten, Anti-de Sitter space and holography, Adv. Theor. Math. Phys. **2**, 253 (1998).

[4] L. Susskind, The world as a hologram, J. Math. Phys. (N.Y.) **36**, 6377 (1995).

[5] S. A. Hartnoll, Lectures on holographic methods for condensed matter physics, Classical Quantum Gravity **26**, 224002 (2009).

[6] H. S. M. Coxeter, Regular honeycombs in hyperbolic space, in *Proceedings of the International Congress of Mathematicians 1954, Amsterdam* (North-Holland Publishing, Amsterdam, 1956), Vol. 3.

[7] W. Magnus, Noneuclidean Tesselations and Their Groups (Academic Press, New York, 1974).

[8] R. C. Brower, C. V. Cogburn, A. L. Fitzpatrick, D. Howarth, and C.-I. Tan, Lattice setup for quantum field theory in AdS_2, Phys. Rev. D **103**, 094507 (2021).

[9] M. Asaduzzaman, S. Catterall, J. Hubisz, R. Nelson, and J. Unmuth-Yockey, Holography on tessellations of hyperbolic space, Phys. Rev. D **102**, 034511 (2020).

[10] M. Asaduzzaman, S. Catterall, J. Hubisz, R. Nelson, and J. Unmuth-Yockey, Holography for Ising spins on the hyperbolic plane, Phys. Rev. D **106**, 054506 (2022).

[11] R. C. Brower, C. V. Cogburn, and E. Owen, Hyperbolic lattice for scalar field theory in AdS_3, Phys. Rev. D **105**, 114503 (2022).

[12] P. Bienias, I. Boettcher, R. Belyansky, A. J. Kollar, and A. V. Gorshkov, Circuit Quantum Electrodynamics in Hyperbolic Space: From Photon Bound States to Frustrated Spin Models, Phys. Rev. Lett. **128**, 013601 (2022).

[13] A. J. Kollár, M. Fitzpatrick, P. Sarnak, and A. A. Houck, Line-graph lattices: Euclidean and non-euclidean flat bands, and implementations in circuit quantum electrodynamics, Commun. Math. Phys. **376**, 1909 (2019).

[14] A. J. Kollár, M. Fitzpatrick, and A. A. Houck, Hyperbolic lattices in circuit quantum electrodynamics, Nature (London) **571**, 45 (2019).

[15] I. Boettcher, P. Bienias, R. Belyansky, A. J. Kollár, and A. V. Gorshkov, Quantum simulation of hyperbolic space with circuit quantum electrodynamics: From graphs to geometry, Phys. Rev. A **102**, 032208 (2020).

[16] S. Yu, X. Piao, and N. Park, Topological Hyperbolic Lattices, Phys. Rev. Lett. **125**, 053901 (2020).

[17] P. M. Lenggenhager, A. Stegmaier, L. K. Upreti, T. Hofmann, T. Helbig, A. Vollhardt, M. Greiter, C. H. Lee, S. Imhof, H. Brand, T. Kießling, I. Boettcher, T. Neupert, R. Thomale, and T. Bzdušek, Simulating hyperbolic space on a circuit board, Nat. Commun. **13**, 4373 (2022).

[18] A. Chen, H. Brand, T. Helbig, T. Hofmann, S. Imhof, A. Fritzsche, T. Kießling, A. Stegmaier, L. K. Upreti, T. Neupert, T. Bzdušek, M. Greiter, R. Thomale, and I. Boettcher, Hyperbolic matter in electrical circuits with tunable complex phases, arXiv:2205.05106.

[19] M. Axenides, E. G. Floratos, and S. Nicolis, Modular discretization of the AdS_2/CFT_1 holography, J. High Energy Phys. 02 (2014) 109.

[20] M. Axenides, E. Floratos, and S. Nicolis, The arithmetic geometry of AdS_2 and its continuum limit, SIGMA **17**, 004 (2021).

[21] E. Gesteau, M. Marcolli, and S. Parikh, Holographic tensor networks from hyperbolic buildings, J. High Energy Phys. 10 (2022) 169.

[22] P. Breitenlohner and D. Z. Freedman, Positive energy in anti-de sitter backgrounds and gauged extended supergravity, Phys. Lett. **115B**, 197 (1982).

[23] P. Breitenlohner and D. Z. Freedman, Stability in gauged extended supergravity, Ann. Phys. (N.Y.) **144**, 249 (1982).

[24] For a concise review of the BF bound, see Ref. [25], page 195.

[25] M. Ammon and J. Erdmenger, *Gauge/Gravity Duality: Foundations and Applications* (Cambridge University Press, Cambridge, England, 2015).

[26] C. H. Lee, S. Imhof, C. Berger, F. Bayer, J. Brehm, L. W. Molenkamp, T. Kiessling, and R. Thomale, Topolectrical circuits, Commun. Phys. **1**, 39 (2018).

[27] E. Zhao, Topological circuits of inductorsand capacitors, Ann. Phys. (Amsterdam) **399**, 289 (2018).

[28] We denote (3) as Klein-Gordon equation, although it does not contain a time derivative. We consider it to be fully defined by the metric (1) and the Laplace-Beltrami operator.

[29] See Supplemental Material at http://link.aps.org/supplemental/10.1103/PhysRevLett.130.091604 for details on the analytical computations and numerical simulations, which include Refs. [30–36].

[30] M. Abramowitz and I. Stegun, *Handbook of Mathematical Functions: With Formulas, Graphs, and Mathematical Tables*, Applied Mathematics Series (Dover Publications, New York, 1965).

[31] L. Abbott and S. Deser, Stability of gravity with a cosmological constant, Nucl. Phys. **B195**, 76 (1982).

[32] S. S. Gubser, M. Heydeman, C. Jepsen, M. Marcolli, S. Parikh, I. Saberi, B. Stoica, and B. Trundy, Edge length dynamics on graphs with applications to p-adic AdS/CFT, J. High Energy Phys. 06 (2017) 157.

[33] J. Ambjørn, A. Goerlich, J. Jurkiewicz, and R. Loll, Nonperturbative quantum gravity, Phys. Rep. **519**, 127 (2012).

[34] R. Loll, Quantum gravity from causal dynamical triangulations: A review, Classical Quantum Gravity **37**, 013002 (2020).

[35] K. E. Atkinson, *An Introduction to Numerical Analysis*, 2nd ed. (John Wiley & Sons, New York, 1989).

[36] W. H. Press, S. A. Teukolsky, W. T. Vetterling, and B. P. Flannery, *Numerical Recipes 3rd Edition: The Art of Scientific Computing*, 3rd ed. (Cambridge University Press, Cambridge, England, 2007).

[37] I. R. Klebanov and E. Witten, AdS/CFT correspondence and symmetry breaking, Nucl. Phys. **B556**, 89 (1999).

[38] L. Mezincescu and P. Townsend, Stability at a local maximum in higher dimensional anti-deSitter space and applications to supergravity, Ann. Phys. (N.Y.) **160**, 406 (1985).

[39] D. B. Kaplan, J.-W. Lee, D. T. Son, and M. A. Stephanov, Conformality lost, Phys. Rev. D **80**, 125005 (2009).

[40] S. Katok, *Fuchsian Groups*, Chicago Lectures in Mathematics (University of Chicago Press, Chicago, 1992).

[41] I. Boettcher, A. V. Gorshkov, A. J. Kollár, J. Maciejko, S. Rayan, and R. Thomale, Crystallography of hyperbolic lattices, Phys. Rev. B **105**, 125118 (2022).

[42] H. S. M. Coxeter, The trigonometry of hyperbolic tessellations, Can. Math. Bull. **40**, 158 (1997).

[43] N. H. Asmar, *Partial Differential Equations with Fourier Series and Boundary Value Problems* (Courier Dover Publications, New York, 2016).

[44] K. W. Morton and D. F. Mayers, *Numerical Solution of Partial Differential Equations: An Introduction* (Cambridge University Press, Cambridge, England, 2005).

[45] O. G. Ernst and M. J. Gander, Why it is difficult to solve Helmholtz problems with classical iterative methods, *Numerical Analysis of Multiscale Problems*, edited by I. Graham, T. Hou, O. Lakkis, and R. Scheichl, Lecture Notes in Computational Science and Engineering Vol. 83 (Springer, Berlin, Heidelberg, 2012), p. 325, 10.1007/978-3-642-22061-6.

[46] Y. Saad, *Iterative Methods for Sparse Linear Systems* (SIAM, Philadelphia, 2003).

[47] Y. Saad and M. H. Schultz, GMRES: A generalized minimal residual algorithm for solving nonsymmetric linear systems, SIAM J. Sci. Stat. Comput. **7**, 856 (1986).

[48] H. A. Van der Vorst, Bi-CGSTAB: A fast and smoothly converging variant of Bi-CG for the solution of nonsymmetric linear systems, SIAM J. Sci. Stat. Comput. **13**, 631 (1992).

[49] M. Schrauth, Y. Thurn, F. Dusel, F. Goth, D. Herdt, and J. S. E. Portela, The HYPERTILING project, www.hypertiling.de, 10.5281/zenodo.7559394 (2023).

[50] J. Dong, V. Juričić, and B. Roy, Topoelectric circuits: Theory and construction, Phys. Rev. Res. **3**, 023056 (2021).

[51] Note that the time t is an auxiliary parameter introduced to parametrize the oscillatory eigenmodes of the circuit and is not related to the total energy (7) of the gravitational system.

[52] T. Kotwal, F. Moseley, A. Stegmaier, S. Imhof, H. Brand, T. Kießling, R. Thomale, H. Ronellenfitsch, and J. Dunkel, Active topolectrical circuits, Proc. Natl. Acad. Sci. U.S.A. **118**, e2106411118 (2021).